
**STATE RESEARCH CENTER OF RUSSIA**

**INSTITUTE FOR HIGH ENERGY PHYSICS**

IHEP 2003-4

V.I. Garkusha, F.N. Novoskoltsev, V.N. Zapolsky, V.G. Zarucheisky

# CALCULATED CHARACTERISTICS OF THE SEPARATED KAON BEAM FOR OKA EXPERIMENT AT THE U-70 ACCELERATOR

Protvino 2003

UDK 539.12.183 M–24

**Abstract**

Garkusha V.I. et al. Calculated Characteristics of the Separated Kaon Beam for OKA Experiment at the U-70 Accelerator: IHEP Preprint 2003-4. – Protvino, 2003. – p. 13, figs. 11, tables 3, refs.: 11.

The design of the beam optics for the separated kaon beam, which is under construction at the 70 GeV IHEP accelerator, is described. Calculated characteristics of the separated beam are presented along with estimations of hadron and muon backgrounds.

**Аннотация**

Гаркуша В.И. и др. Расчетные характеристики пучка сепарированных каонов для эксперимента ОКА на ускорителе У70: Препринт ИФВЭ 2003-4. – Протвино, 2003. – 13 с., 11 рис., 3 табл., библиогр.: 11.

Приводится описание оптики канала сепарированных каонов, сооружаемого на 70-ГэВ ускорителе ИФВЭ. Представлены расчетные характеристики сепарированного пучка, а также оценки адронного и мюонного фонов.

## 1. Introduction

This paper describes results of the beam optics design for the separated kaon beam to be constructed at the 70 GeV IHEP proton synchrotron U-70. The beam is intended for direct CP-violation searches in $K^{\pm}$ decays, as well as for other experiments in the context of the experimental program OKA [1].

The two-cavity superconducting RF separator, developed and constructed at KfK, Karlsruhe, and operated during 1978–1981 in 10–40 GeV/c beams for the Ω-spectrometer at CERN [2], will be used for separation of kaons in the considered beam-line. In 1998 this separator was delivered to IHEP and is under testing now. Main parameters of the separator, affecting on the beam optics design, are given in Table 1.

Table 1. Main parameters of the RF separator.

| | |
|---|---|
| Frequency, $f$ | 2865.7 MHz |
| Wave length, $\lambda$ | 0.1046 m |
| Cavity length, $l$ | 2.74 m |
| Aperture, $d$ | 39.8 mm |
| Deflecting field, $E$ | $\leq$ 1.2 MV/m |
| Windows (50 $\mu$m Kapton) | 2+2 per cavity |

The new beam-line (21K) will be located in the U-70 gallery (Figure 1), which already houses some beams produced from the fast and slow extracted primary proton beam. They are the multi-purpose secondary beam (22) and two neutrino beams (8 and 23) with wide and narrow energy spread, respectively.

The design of optics for the separated beam was based on the existing magnetic equipment, which was developed more than 30 years ago for particle beams of U-70. It contains mainly 2 m quadrupoles with 200 mm aperture (20K200 type), small number of 1 m quadrupoles (20K100 type), 3 m dipole magnets with 350×150 mm$^2$ aperture (СП032 type) and 4 m dipole magnets with 330×100 mm$^2$ aperture (СП129 type).

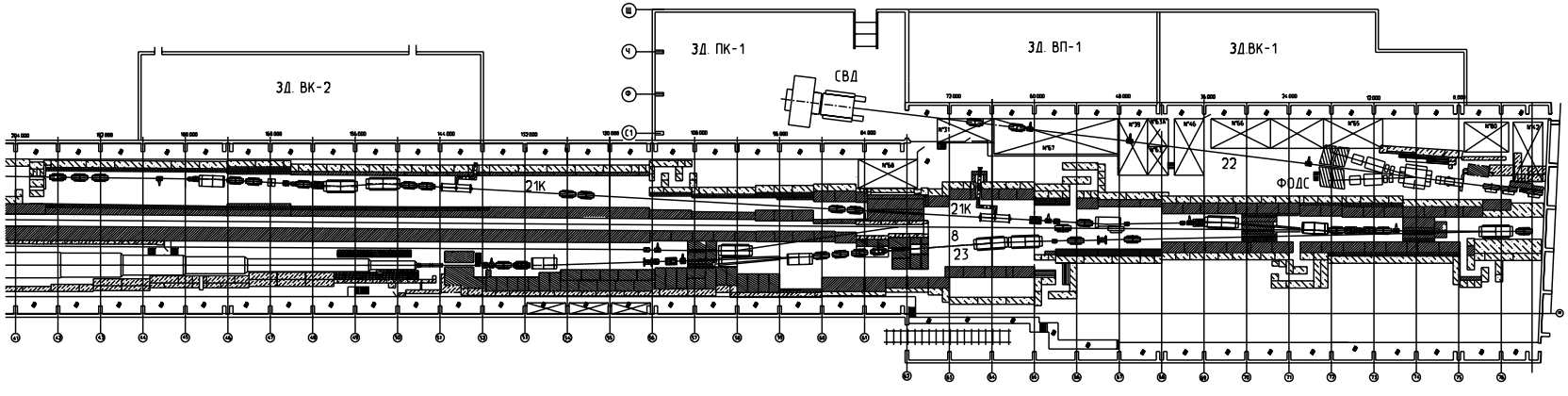


Fig. 1. The layout of the IHEP separated kaon beam (beam-line 21K).

## 2. Two-Cavity Separation

In case of two-cavity separation all particles with momentum $p$ passing the first cavity are deflected in the transverse direction according to $y' = A\sin(\omega t)$, where $A = eEl/pc$ and $\omega t$ is the phase of a particle with respect to the cavity wave. If the optics between two cavities has $(\pm 1)$ transformation matrix and deflecting fields in both cavities are equal, the phase of the second cavity may be tuned to cancel the deflection of unwanted particles $m_1$. For the (–1) optics between cavities the total deflection of the particle $m_2$ is:

$$y' = -A\sin(\omega t) + A\sin(\omega t + \tau_{21}) = D_2\cos(\omega t + \tau_{21}/2),$$

where $D_2 = 2A\sin(\tau_{21}/2)$ is the amplitude of the deflection and $\tau_{21}$ is the phase shift between particles $m_2$ and $m_1$ at the distance $L$ between two cavities of the RF separator:

$$\tau_{21} = 2\pi\frac{L}{\lambda}\beta_2\left(\frac{1}{\beta_2} - \frac{1}{\beta_1}\right) \overset{pc \gg \mathcal{E}_0}{\longrightarrow} \pi\frac{L}{\lambda}\frac{\mathcal{E}_{02}^2 - \mathcal{E}_{01}^2}{(pc)^2}.$$

Deflection amplitudes of kaons and protons at the cancelled deflection of pions for the considered beam-line with $L = 76.273$ m are shown in Figure 2. To obtain a $K^+$ separated beam, it is necessary to reject protons too. Besides the main operational mode at 12.50 GeV/c, when the protons are 720° out of pions ($\tau_{K\pi} = 187°$), this is also achievable at 17.68 GeV/c ($\tau_{p\pi} = 360°$, $\tau_{K\pi} = 94°$) and at 10.21 GeV/c ($\tau_{p\pi} = 1080°$, $\tau_{K\pi} = 280°$). Separation at lower values of momenta are senseless due to a large decay of kaons at the given length of the beam-line.

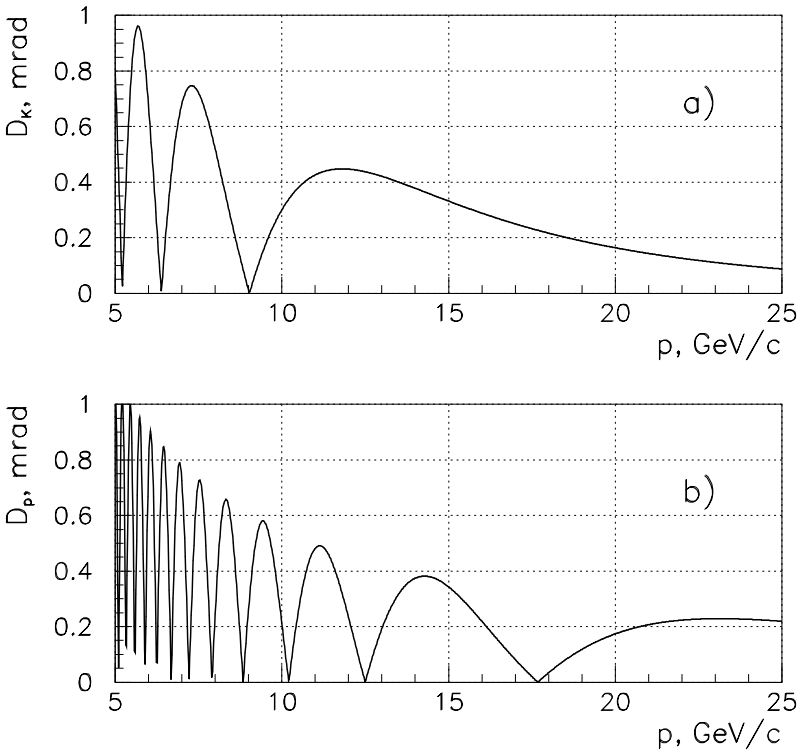


Fig. 2. Angular deflection amplitudes of kaons (a) and protons (b) after two cavities of the RF separator in the considered beam optics design for a 1 MV/m deflecting field.

One should note, that given above expressions are valid for monochromatic ($\Delta p/p \to 0$) beams. In reality, for the beam with a few percent $\Delta p/p$, the phase shift between two kinds of particles at the distance $L$ is:

$$\tau_{21} \simeq \tau_{21}^0 \left(1 - 2\frac{\Delta p}{p}\right),$$

where $\tau_{21}^0$ is the phase shift for the beam with $\Delta p/p = 0$. It is most pronounced for rejection of protons in case of separation with large $\tau_{p\pi}$, e.g. for the considered in this paper beam $\Delta\tau_{p\pi} = \tau_{p\pi} - \tau_{p\pi}^0$ reaches $\sim 60^\circ$ for particles with $\Delta p/p \sim 3\%$ in case of $p = 10.21$ GeV/c and, as a result, their deflection will not be cancelled completely.

Furthermore, due to the slip of low momentum particles (primarily protons) with respect to the wave, their angular deflection after passing a cavity of the RF separator will be:

$$y' = A\frac{\sin(\varphi/2)}{\varphi/2}\sin(\omega t + \varphi/2),$$

where $\varphi \simeq \pi\frac{l}{\lambda}\frac{\mathcal{E}_0^2}{(pc)^2}$ is the particle phase shift at the length of the cavity; i.e. smaller than that for relativistic particles.

Both these peculiarities of the RF separation were taken into account in the presented below results of beam simulations.

## 3. Beam Optics

The optics of the RF separated beam, consisting of three different special-purpose sections, is shown in Figure 3. The total length of the beam-line between the production target and the entrance of the decay region (6 m downstream the last quadrupole of a beam-line) is equal to 202 m. The optics is optimized to produce a 12.5 GeV/c separated kaon beam, while the maximal allowable momentum of the beam is about 20 GeV/c. The beam optics calculations were made using the program TRANSPORT [3].

### 3.1. First Section

The 70 GeV/c primary proton beam with intensity up to $10^{13}$ per 1.8–2.0 s spill every 9 s strikes the target, which is the 3.5 mm high and 0.5 m long air-cooled aluminum plate (Section 4). The proton beam spot size in the target is $\sigma_x \times \sigma_y = 1.0 \times 0.8$ mm$^2$.

Four quadrupoles Q1–Q4 are used to capture the charged secondaries emerging from the target around 0 mrad production angle. The angular acceptance, namely $\pm 10$ mrad horizontally and $\pm 2.2$ mrad vertically for the separated beam, is selected with help of two collimators placed just before Q1 (C1) and between Q2 and Q3 (C2)[1].

First set of quadrupoles is followed by the momentum defining section, consisting of three dipole magnets B1–B3, quadrupole Q5 and horizontal collimator C3. After B1 most of secondaries, which are beyond the acceptance of the beam-line, and non-interacting primary protons are dumped in a 4 m massive unadjustable collimator (DUMP). At the momentum dispersion $R_{16} = 8.4$ mm per 1% $\Delta p/p$ and magnification $R_{11} = 3.5$, the collimator C3 with opening range $\pm 10$ mm provides the momentum resolution $\Delta p/p = \pm 2.0\%$. The maximal allowed momentum bite of the beam is about $\pm 6\%$ at the fully opened C3.

[1] In the unseparated mode the angular acceptance of the beam in the vertical plane may reach $\pm 5$ mrad.

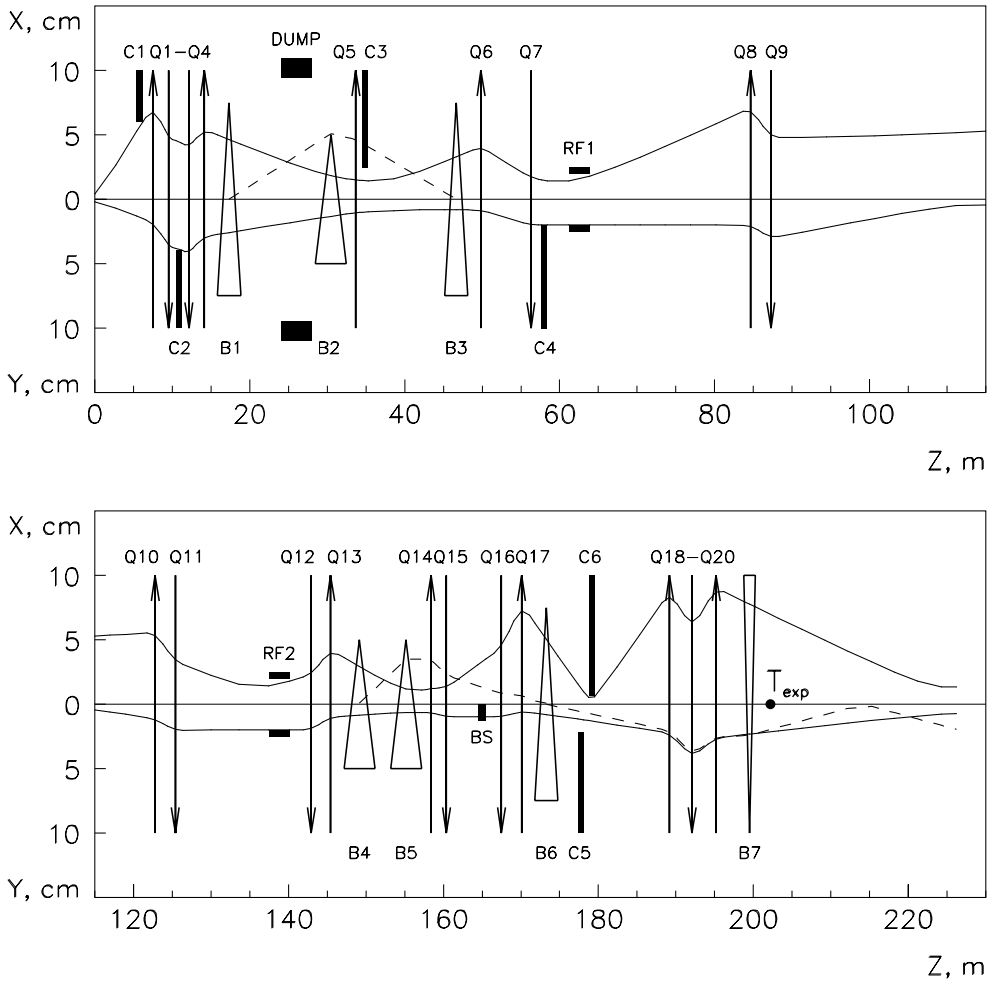


Fig. 3. The optics of the separated kaon beam. Beam envelopes are given for $\Delta p/p = 0$ in case when the beam is focused towards the decay region. The separator is turn off. The dispersion is shown for $\Delta p/p = 5\%$.

The doublet Q6–Q7 forms the beam in the first cavity (RF1) of the separator. The angular magnification in the vertical plane $R_{44}$ is 0.1, so the 2.2 mrad angle at the production target transforms into 0.22 mrad angle in RF1. This angle is only two times smaller than the maximal deflection providing by two cavity separator with $E = 1.0$ MV/m for the 12.5 GeV/c beam, and therefore requires an elaborate minimization of the second order effects contribution to the vertical divergence. The collimator C4 with opening range $\pm 20$ mm in the vertical plane cuts the secondaries which are out of the aperture of RF cavities. In the horizontal plane the beam is matched with an acceptance of the remaining part of a beam optics, including limitations due to the relatively small aperture of RF cavities.

### 3.2. Intercavity Section

To satisfy the requirements of two-cavity separation, this part of the beam optics provides (–1) transformation of a beam in the vertical plane between centers of RF1 and RF2. Four quadrupoles Q8–Q11 with equal gradients, which form two cells of a FODO structure with

the 90° phase advance per cell in each plane, give a completely (–1) transformation in both planes ($R_{12} = R_{21} = 0, R_{34} = R_{43} = 0$). This variant of intercavity optics provides also an adequate acceptance for the beam in the horizontal plane and minimal chromatic aberrations in the vertical plane.

### 3.3. Final Section

Quadrupoles Q12–Q15 act so that the beam size at the beam stopper (BS) in the vertical plane is proportional in the first order to the angular divergency of the beam after RF2 ($R_{33} = R_{44} = 0$). In this case unwanted particles (pions and protons), whose deflection obtained in RF1 is cancelled in RF2, are dumped in the beam stopper, while the wanted particles (kaons) with about double deflection after two cavities of the separator partially bypass the beam stopper. The central part of the kaon beam is also intercepted by the beam stopper. Actually, due to: chromatic aberrations in a beam, incompletely cancelled deflection for particles with $\Delta p/p \neq 0$, not full absorption in the material of the beam stopper and collimators, as well as multiple scattering in Kapton windows, a number of unwanted particles bypasses the beam stopper hand in hand with wanted particles giving a hadron background in the separated beam.

Quadrupoles Q16–Q17 provides the beam focusing in collimators C5 and C6. It is important to note, that the wanted particles have a zero dispersion in the horizontal collimator C6 with relatively small opening range ±6 mm, while the dispersion of unwanted particles emerging from the beam stopper is equal to 2.5 mm per 1% $\Delta p/p$ at this point, and it helps to reduce the hadron background.

Last three quadrupoles Q18–Q20 provide adequate beam spot sizes at the various parts of the experimental set-up, i.e. either to focus the beam on the target located 6 m downstream Q20, or to form the beam towards the decay region.

Since the middle plane of the experimental set-up is ∼70 cm higher than the axis of the beam, the final section of the beam-line includes two vertical bends. The B6 dipole, rotated by ∼31° around its longitudinal axis, realizes the first vertical bend (26 mrad) of the beam. The beam is bent back to the horizontal plane by the a 1.5 m dipole B7 with large aperture, which will be also used for measurements of the momentum of individual particles. An incomplete compensation of the dispersion for reasons of space leads to somewhat increase of the vertical beam size in the experimental area.

## 4. Calculations of Particle Fluxes

Calculations of particle fluxes were made using the Monte Carlo program HALO [4] adapted for simulations of the separated beam. Besides insertion of some specific elements (deflectors of the RF separator and beam stopper), it includes also the tracking of secondaries, which hit the beam stopper, collimators and vacuum pipe walls. The energy loss, absorption and multiple scattering of secondaries are taken into account, but tertiary particles are not generated. This approach allows estimations of a hadron background without substantial time consumption inherent in computer programs simulating a wider range of physical effects.

Secondary particle yields from a target were calculated using the parametrization of inclusive invariant cross-sections, proposed by M.Bonesini et al. [5] for particle production, measured in p-Be interactions with 400 GeV/c and 450 GeV/c primary protons at CERN [6,7]. The primary proton beam with Gaussian distributions in both transverse directions hits the production target

of chosen dimensions and material. Secondaries are generated in the target along primary proton trajectories according to distribution of proton interaction points. The path of secondaries in the target was calculated in order to estimate the probability for these particles leaving the target without interaction. Protons missing a target in Gaussian tails were not traced downstream the beam-line.

Because this simple reabsorption model neglects production of tertiary particles, their contribution due to interaction of higher energy secondaries (mainly protons) was added for relatively thin (2–4 mm) plate targets as[2]:

$$\widetilde{N}(x, p_T) = N(x, p_T)(1 + A_h(x)(1 - e^{-L/2\lambda_p})),$$

where $L$ is the length of a target and $\lambda_p$ is the nuclear interaction length of protons. An approximation of $A_h(x)$ as a function of $x = p/p_{inc}$ is given in [5] for particle production in the forward direction from the 2 mm thick and 100 mm long beryllium plate target.

Scaling of the used production model to a different target material is based on the relation between the particle yield and the inclusive invariant production cross-section:

$$\frac{d^2N}{dpd\Omega} = \left(E\frac{d^3\sigma}{dp^3}\right)\frac{p^2}{\sigma_0 E},$$

where $\sigma_0$ is the absorption cross-section of protons in a target material. The inclusive invariant cross-section and absorption cross-section for hadron-nuclei interactions $pA \to hX$ depend on the atomic mass number $A$ as:

$$\left(E\frac{d^3\sigma}{dp^3}\right)_{A_2} = \left(\frac{A_2}{A_1}\right)^{\alpha(x_F)}\left(E\frac{d^3\sigma}{dp^3}\right)_{A_1},$$

$$(\sigma_0)_{A_2} = \left(\frac{A_2}{A_1}\right)^{\alpha_0}(\sigma_0)_{A_1},$$

where $\alpha(x_F) = 0.74 - 0.55x_F + 0.26x_F^2$ and does not depend on the type of secondary particle [8], $x_F \simeq 2p_L^*/\sqrt{s}$, $p_L^*$ and $\sqrt{s}$ are the longitudinal momentum of secondary particle and the total energy in the centre-of-mass frame, and $\alpha_0 \simeq 0.72$ for relatively wide range (60–280 GeV/c) of incident proton momenta [9]. By this means, the rescale of particle yields from p-Be interactions to particle yields from interactions of protons with different materials (for example, aluminum) was done following to:

$$\left(\frac{d^2N}{dpd\Omega}\right)_{Al} = \left(\frac{A_{Al}}{A_{Be}}\right)^{\alpha(x)-\alpha_0}\left(\frac{d^2N}{dpd\Omega}\right)_{Be}.$$

Figure 4 shows the fluxes of 12.5 GeV/c $K^+$'s before RF1 calculated as functions of a target length for different target materials. All targets are 3.5 mm thick and 25 mm wide plates located so that the center of target coincide with focal point of a beam optics ($Z$=0 in Figure 3). Despite of ∼10% gain in kaon flux, which gives the beryllium target with respect to the aluminum one, an aluminum was chosen as a target material due to its safe machining and easy in operation. The general view of the air cooled aluminum target is shown in Figure 5.

[2]Contribution of tertiary particles essentially depends on transverse sizes and the length of a target, i.e. on the probability for the secondary particle to interact before it escapes from the target. Therefore, the use of Monte Carlo programs even with rough simulations of secondary interactions is more preferable for prediction of tertiary contribution in the general case.

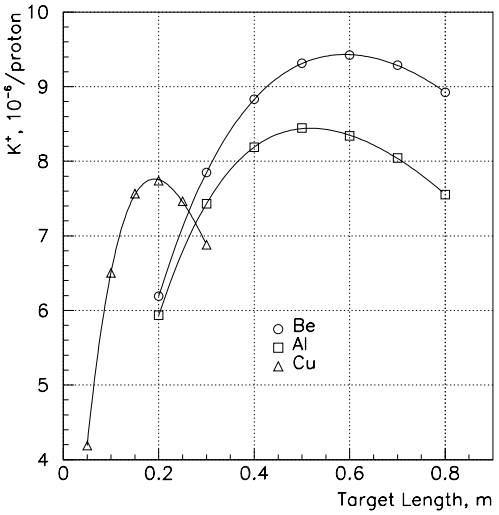


Fig. 4. Fluxes of 12.5 GeV/c kaons before RF1 as functions of a target length for different target materials.

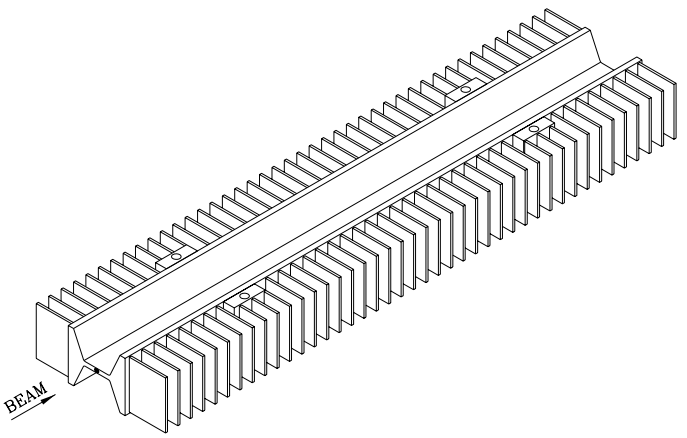


Fig. 5. The general view of the 0.5 m aluminum target.

## 5. Main Characterictics of Separated Beams at the End of the Beam-Line

Momentum and space distributions of the separated beam at the entrance of the decay region ($Z$ = 202 m) are shown in Figures 6 and 7 for the opening range of momentum slit C3 equal to ±24 mm and for the 1 MV/m deflecting field in both cavities of the RF separator. The r.m.s. width of momentum spread is equal to 1.5% $\Delta p/p$, and the size of the beam spot is $\sigma_x \times \sigma_y = 34 \times 17$ mm$^2$. Due to the convergence of the beam its r.m.s. sizes 24 m downstream are 7×11 mm$^2$, where ∼87% of particles are inside of the 30×30 mm$^2$ area. Although a number of wanted particles is removed from the beam by the beam stopper, the proper optimization of the optics after the beam stopper prevents arising of a hole in transverse beam distributions along the decay region (Figure 7).

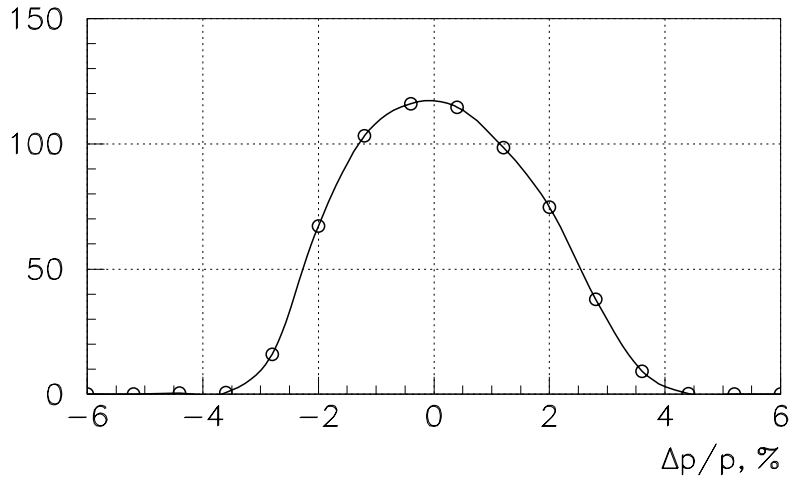


Fig. 6. The momentum distribution of the separated kaon beam at the entrance of the decay region.

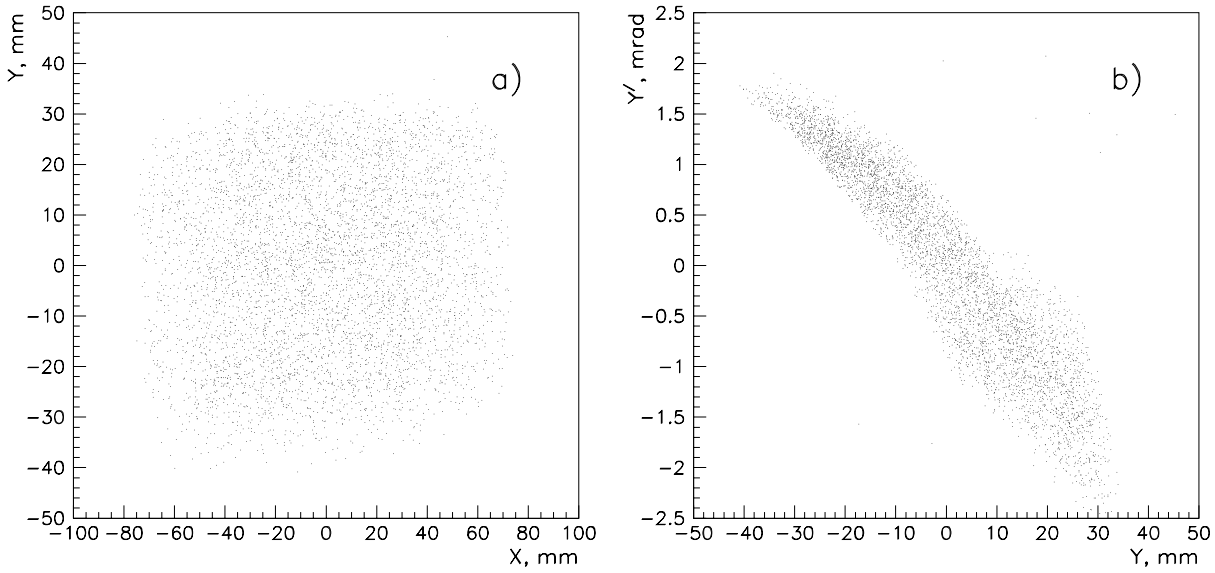


Fig. 7. The cross-section (a) and the vertical phase space (b) of the separated kaon beam at the entrance of the decay region.

The intensity of the separated beam, as well as contamination of a beam by unwanted particles (hadron background) essentially depends on beam stopper sizes, but if the intensity is determined mainly by the thickness of the beam stopper, then the background is determined by its length too. Two processes, an absorption and an energy loss, are "responsible" for removing of unwanted particles from a beam. To provide a 400 times decrease of pion flux[3] due to absorption in material, the iron beam stopper should be about 1.25 m length. At the same time, the average energy loss of particles even in the 1 m beam stopper is about 10% for the 12.5 GeV/c beam, that is quite enough to remove these particles from a beam-line acceptance by means of dipole B6 and collimator C6 (Figure 3).

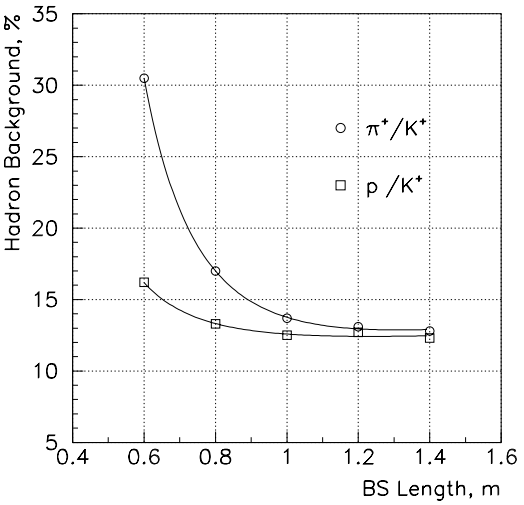


Fig. 8. The hadron background at the entrance of the decay region as a function of the length of the iron beam stopper for the 12.5 GeV/c tune of separated beam. The thickness of the beam stopper is equal to 28 mm.

[3]The flux of unwanted particles (pions and protons) at the entrance of decay region in the 12.5 GeV/c unseparated beam is ∼100 times higher than the kaon flux. To limit the hadron background in the separated beam by the value of ≤50%, the beam stopper with efficiency ∼0.5 should be long enough to reduce the flux of unwanted particles by a factor of ≥400.

Figure 8 shows the dependence of hadron background on the length of the iron beam stopper for the main operational mode (tune) of the separated beam. As it follows from these plots, there is no need to use the beam stopper with the length larger than 1.2 m. Taking into account, that approximately the same dependence take place for the copper beam stopper too, all subsequent calculations were made for the 1.2 m iron beam stopper.

### 5.1. Kaon Beams

The dependence of kaon intensity and hadron background at the entrance of the decay region on the beam stopper thickness are shown in Figure 9 for the 12.5 GeV/c tune of beam. An optimal thickness of the beam stopper is in the range 26–30 mm, i.e. the smaller thickness causes the catastrophic increase of hadron background due to unwanted particles bypassing the beam stopper together with wanted kaons, while at larger thickness the hadron background decreases slowly than the intensity of kaons.

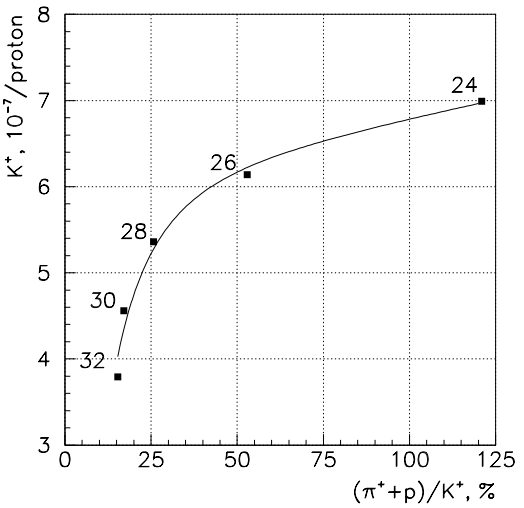


Fig. 9. The flux of kaons at the entrance of the decay region as a function of the hadron background for the 12.5 GeV/c tune of separated beam. Numbers along-side the plots give the thickness of the beam stopper.

Table 2. Hadron fluxes per incident proton at the entrance of the decay region for separated kaon beams.

| $p$, GeV/c | 10.2 | 12.5 | 17.7 |
|---|---|---|---|
| BS thickness, mm | 29 | 28 | 26 |
| BS efficiency | 0.22 | 0.38 | 0.11 |
| $K^+$ | – | $5.4\times10^{-7}$ | $3.5\times10^{-7}$ |
| $\pi^+$ | – | $7.0\times10^{-8}$ | $1.3\times10^{-7}$ |
| $p$ | – | $6.8\times10^{-8}$ | $9.5\times10^{-8}$ |
| $(\pi^+ + p)\,/\,K^+$, % | – | 26 | 64 |
| $K^-$ | $7.5\times10^{-8}$ | $2.3\times10^{-7}$ | $1.1\times10^{-7}$ |
| $\pi^-$ | $4.4\times10^{-8}$ | $4.2\times10^{-8}$ | $6.0\times10^{-8}$ |
| $\tilde{p}$ | $1.5\times10^{-8}$ | $2.0\times10^{-9}$ | $1.0\times10^{-9}$ |
| $(\pi^- + \tilde{p})\,/\,K^-$, % | 79 | 19 | 55 |

The other results of beam simulations for the kaon separated beams are summarized in Table 2. As stated above, the separated beam of kaons is available also at 10.2 and 17.7 GeV/c, but, due to the smaller deflection amplitude (Section 2), the efficiencies of the beam stopper for these separation modes are significantly lower than that for the main operational mode at 12.5 GeV/c. Moreover, at 10.2 GeV/c the phase shift between protons and pions at the distance between two cavities of separator increases up to $6\pi$, and, because of the finite value of $\Delta p/p$, the deflection of protons after two cavities is not cancelled completely. This causes a large background of protons in the $K^+$ separated beam, which can not be eliminated by an increase of the beam stopper thickness. Other than these the separation of kaons at low momenta is limited also by multiple scattering of unwanted particles in Kapton windows before and after each cavity. The multiple scattering in Kapton windows varies inversely with momentum and gives about one half of the hadron background in the kaon beam even at 12.5 GeV/c.

### 5.2. Antiproton Beams

According to separation curves shown in Figure 2, the considered beam-line with two-cavity separator can also be used for producing of separated antiproton beams. Results of the beam simulation for some possible tunes of the antiproton separated beam are given in Table 3. The separation of antiprotons is not limited by the low momenta due to the decay of wanted particles, as in the case of kaon beams. On the other hand, similar to the separated kaon beams the multiple scattering of pions in Kapton windows leads to large background of unwanted particles at low momenta tunes.

Table 3. Hadron fluxes per incident proton at $Z = 202$ m for separated antiproton beams. The thickness of the beam stopper is equal to 28 mm.

| $p$, GeV/c | 6.45 | 7.54 | 9.43 | 14.3 |
|---|---|---|---|---|
| BS efficiency | 0.53 | 0.56 | 0.51 | 0.27 |
| $\tilde{p}$ | $3.5\times10^{-7}$ | $4.9\times10^{-7}$ | $5.7\times10^{-7}$ | $3.5\times10^{-7}$ |
| $\pi^-$ | $2.8\times10^{-7}$ | $1.8\times10^{-7}$ | $8.7\times10^{-8}$ | $4.0\times10^{-8}$ |
| $K^-$ | $4.5\times10^{-9}$ | $6.5\times10^{-8}$ | $1.0\times10^{-8}$ | $2.1\times10^{-7}$ |
| $(\pi^- + K^-)\,/\,\tilde{p}$, % | 81 | 51 | 17 | 71 |

## 6. Muon Background

The muon background at the experimental set-up, defined as the rate of muons in the 1 m radius surface located 24 m downstream the entrance of decay region, was preliminary studied using HALO. For the 12.5 GeV/c tune of beam the total flux of muons in this surface is factor 2.7 larger than the flux of separated kaons at the entrance of decay region. As found, the main contribution to muon background ($\sim$95%) gives the decay of pions in the beam-line upstream the beam stopper. Radial distribution of these muons at the experimental set-up (Figure 10) shows that about 30% of muons occupies the nearest to beam axis area with a radius of 50 mm. Taking into account that momentum distribution of near-axis muons is very close to momentum distribution of the separated kaon beam, it is difficult to attain a noticeable decrease of this component of muon background.

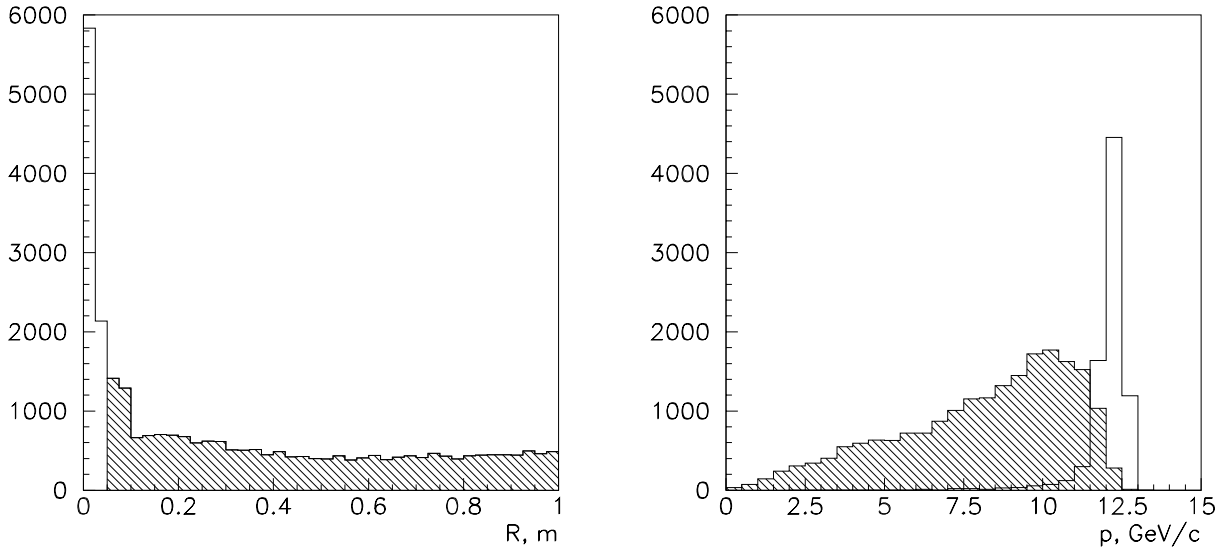


Fig. 10. Radial (left) and momentum (right) distributions of the $\mu^+$ background 24 m downstream the entrance of the decay region for the 12.5 GeV/c tune of beam. The unshaded parts of histograms correspond to muons from the near-axis area with $R \leq 50$ mm.

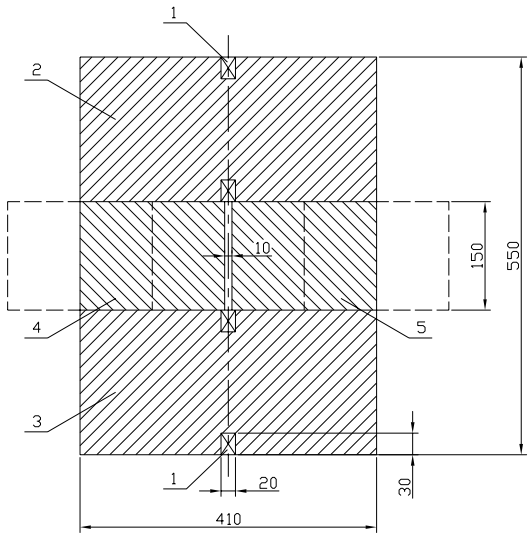


Fig. 11. The cross-section of the horizontal magnetic collimator. 1 – exciting coils; 2, 3 – unmovable blocks; 4, 5 – movable blocks.

Similar to muon beams [10], the background of muons outside the near-axis area can be reduced with help of adjustable magnetic collimators (scrapers) followed by the static magnetised iron shield (see also [11]). In our case the magnetic collimator consists of four 0.75 m steel blocks forming a closed yoke around the beam (Figure 11). Although the range of movement for each movable block is from $-50$ mm up to $+50$ mm (zero position for both blocks corresponds to entirely closed collimator), a toroidal magnetic field with $B \sim 1.2$ T is provided only when movable blocks are on different sides from the exciting coils. The quadrupole stray field between the movable blocks, which is about 0.3 T/m at the $\pm 5$ mm opening range, does not affect at all the hadron beam passing through the collimator.

Calculations show, that the use of three magnetic collimators 3 times reduces the muon flux in the 1 m radius surface excepted the 50 mm radius near-axis area. There are horizontal and vertical collimators just before the beam stopper and the third one as the horizontal collimator C6. An additional 2.5 times decrease of muon flux in this area can provide the 2 m long static magnetised iron shield with transverse sizes $2\times2$ m$^2$ and $B = 0.8$ T located before the last set of quadrupoles Q18–Q20. As a result, the background of muons in the 1 m radius surface decreases up to 70% with 2/3 of this amount inside the 50 mm radius near-axis area.

## References


[1] V.F.Obraztsov, L.G.Landsberg, Prospects for CP violation searches in the future experiment with RF separated $K^{\pm}$ beam at U-70, Nucl. Phys. Proc. Suppl. 99B (2001) 257.

[2] A.Citron et al., The Karlsruhe – CERN superconducting RF separator, Nucl. Instr. and Meth. 164 (1979) 31.

[3] K.L.Brown et al., TRANSPORT. A computer program for designing charged particle beam transport system, CERN 80–04, Geneva, 1980.

[4] Ch.Iselin, HALO. A computer program to calculate muon halo, CERN 74–17, Geneva, 1974.

[5] M.Bonesini et al., On particle production for high energy neutrino beams, Eur. Phys. J. C20 (2001) 13.

[6] H.W.Atherton et al., Precise measurements of particle production by 400 GeV/c protons on beryllium targets, CERN 80–07, Geneva, 1980.

[7] G.Ambrosini et al., Measurement of charged particle production from 450 GeV/c protons on beryllium, Eur. Phys. J. C10 (2001) 605.

[8] D.S.Barton et al., Experimental study of the A dependence of inclusive hadron fragmentation, Phys. Rev. D27 (1983) 2580.

[9] A.S.Carrol et al., Absorption cross sections of $\pi^{\pm}$, $K^{\pm}$, $p$ and $\tilde{p}$ on nuclei between 60 and 280 GeV/c, Phys. Lett. 80B (1979) 319.

[10] N.Doble et al., The upgraded muon beam at the SPS, Nucl. Instr. and Meth. A343 (1994) 351.

[11] A.G.Afonin et al., Universal high intensity beam channel at the IHEP accelerator, Preprint IHEP 90-38, Protvino, 1990.



*Received February 10, 2003*

Препринт отпечатан с оригинала-макета, подготовленного авторами.

В.И.Гаркуша и др.
Расчетные характеристики пучка сепарированных каонов для эксперимента ОКА на ускорителе У70.

Оригинал-макет подготовлен с помощью системы LaTeX.

---

Подписано к печати 03.04.2003. Формат 60 × 84/8.
Офсетная печать. Печ.л. 1.62. Уч.-изд.л. 1.3. Тираж 160. Заказ 39.
Индекс 3649. ЛР №020498 17.04.97.

---

ГНЦ РФ Институт физики высоких энергий
142284, Протвино Московской обл.

Индекс 3649

П Р Е П Р И Н Т 2003–4, И Ф В Э, 2003